

Modeling of a Multi-Stream Injection COIL with Enhanced Mixing Ejectors

Andrew D. Palla¹ and David L. Carroll²
CU Aerospace, Champaign, IL 61820

and

Wayne C. Solomon³
University of Illinois at Urbana-Champaign, Urbana, IL, 61801

Several variants of an ejector mixing nozzle concept for a high-pressure chemical oxygen-iodine laser (COIL) have been experimentally tested. To obtain a better understanding of how much performance enhancement could be expected with increased mixing and to facilitate a larger parametric study we utilized the quasi-1D BLAZE-IV model to simulate these experiments. While computational fluid dynamic (CFD) computations provide critical detailed information about individual flow fields that cannot be obtained with a model such as BLAZE-IV, the computing time required for these CFD calculations inherently limits the number of such computations that can be performed in a reasonable amount of time. Simulation of COIL ejector mixing nozzle experiments required the development of a BLAZE-IV model component capable of treating the simultaneous expansion of multiple mixing streams into a flow region with an initial base area, which is equivalent to the instantaneous introduction of a disparity between the sum of all stream areas and the total internal geometric cross-sectional area. In addition, the model now treats the supersonic expansion of the initially subsonic mixed stream [the $O_2(a^1\Delta)$ stream in the COIL case] which is known to occur downstream of an aerodynamic throat created by the expansion of the higher pressure unmixed streams. A method consistent with all applicable physical laws by which the desired flow conditions are achieved via asymptotic apportionment of the base area was required. A Russian design served as our baseline for the BLAZE-IV modeling calculations performed herein. Comparisons with experimental data and estimations of performance enhancement with faster mixing are presented.

I. Introduction

The chemical oxygen-iodine laser (COIL) was first demonstrated in 1978 [McDermott, 1978]. Since that initial demonstration, COIL technology has undergone numerous improvements [Truesdell, 1992; Zagidullin, 1998; Kodymova, 2007, Endo, 2007]; chemical efficiencies as high as 36-40% using nitrogen diluent have been demonstrated [Rybalkin, 2005]. Much of the COIL technology development to date has focused on the singlet-oxygen generator (SOG). The liquid SOG technology has developed to a fairly mature state. However, much of the work has been performed at relatively low pressures (20-60 Torr) with poor pressure recovery potential. The ability to increase the total pressure and Mach number of the flow, while at the same time maintaining good iodine mixing, cavity kinetics, and generator pressure can have a dramatic impact on the overall system by simplifying the pressure recovery system (by reducing the amount of fluids and weight of ejector hardware) [Boreysho, 2009].

One of the major thrusts in COIL technology in the past decade has been to increase the total pressure of the system for better pressure recovery and to find novel schemes to enhance the iodine mixing in such high pressure systems. Studies by Nikolaev [Nikolaev, 2000; Nikolaev, 2002] and Yang [Yang, 2000] with ejector-mixing nozzles along with detailed modeling [Waichman, 2009; Madden, 2010] have provided important insights into the nozzle

¹ Senior Physicist, CU Aerospace, 301 N. Neil St. – Ste 400, Champaign, IL 61820, Senior Member AIAA.

² President, CU Aerospace, 301 N. Neil St. – Ste 400, Champaign, IL 61820, Fellow AIAA.

³ Professor Emeritus, Univ. of Illinois at Urbana-Champaign, 104 S. Wright, Urbana, IL 61801, Fellow AIAA.

mixing issue and COIL pressure recovery performance. The ejector mixing nozzle concept put forward by the Russian Lebedev Physical Institute research group at Samara [Nikolaev, 2000] appears particularly promising and the design evolved through later work over several years [Zagidullin, 2001; Khvatov, 2002; Hager, 2003; Zagidullin, 2005]. The research discussed herein directly addresses gain generator mixing efficiency for systems having higher pressure recovery potential over the baseline while maintaining singlet oxygen generation and transport efficiency.

The idea of the “Starlet” nozzle concept stems originally from experimental work of Pannu and Johannesen [Pannu, 1976]. Pannu and Johannesen reported results on a series of experiments concerning sonic flow from tubes with V-shaped slots cut into the end of the tube. Our interest in these experiments concerns the flow field generated by the slots that creates two counter-rotating vortices at each notch and that these vortices generate a large outward flow velocity thereby stretching the surface of the mixing interface. This work was then applied to mixing in chemical lasers by Solomon *et al.* [Solomon, 1982] who pioneered the “Star” nozzle concept in which tubes with four notches created a “star” pattern when visualized by laser induced fluorescence techniques. The “Starlet” nozzle concept [Carroll and Solomon, 2009; King, 2010] is a variant design of the source flow ejector mixing nozzle studied by Nikolaev *et al.* in which notches are added to create a high degree of strain or fluid stretch to accelerate the molecular mixing.

To obtain a better understanding of how much performance enhancement could be expected with increased mixing and to facilitate a larger parametric study we utilized the BLAZE-IV model [Palla, 2007a-b; Palla, 2006a-b]. While computational fluid dynamic (CFD) computations such as those performed by [Waichman, 2009] and [Madden, 2010] provide critical detailed information about individual flow fields that cannot be obtained with a model such as BLAZE-IV, the computing time required for these CFD calculations inherently limits the number of such computations that can be performed in a reasonable amount of time. The Russian design [Nikolaev, 2002] serves as our baseline for the BLAZE-IV modeling calculations performed herein. Comparisons with experimental data and estimations of performance enhancement with faster mixing are presented.

II. BLAZE-IV Model

CU Aerospace developed BLAZE-IV [Palla, 2007a-b; Palla, 2006a-b], a multi-physics simulation software package, for physical system analysis. The model was developed using the C++ programming language using modern data abstraction and encapsulation techniques to simplify extensions of the model, at the most basic level, to any problem of interest. BLAZE-IV includes fluid-dynamic, electrodynamic, thermodynamic, plasma-kinetic/kinetic, optical, and elastic solid mechanical modules and is capable of solving multi-dimensional transient and steady-state cell-centered finite-volume problems using both structured and unstructured grids in addition to temporal and spatial marching problems. The model is capable of generating structured rectilinear grids, unstructured grids comprised of triangles (2D) or tetrahedrons (3D) computed using an adaptive Delaunay tessellation scheme, and unstructured grids comprised of n-polygons (2D) or hexahedrons (3D). Additional elements have been added to automate parametric studies by systematic variation of specified parameters. The model has been successfully deployed in a number of widely varied engineering research programs. The research described herein utilized the 1-D spatial marching-mixing model component of the BLAZE-IV model.

The BLAZE-IV 1-D spatial marching-mixing model was designed to perform stream-wise Newton integration of the fluid-dynamics and chemical kinetics of an arbitrary number of mixing internal-flow gas streams. In the default model, the areas of the mixing streams vary as a function of stream-wise location due to internal fluid-dynamics and any stream to stream “area exchange” resulting from mixing. It is assumed that at any axial location the sum of all stream areas is equal to the total internal geometric cross-sectional area. Simulation of COIL mixing experiments described in [Nikolaev, 2002] and [King, 2010] required the development of a model component capable of treating the simultaneous expansion of multiple mixing streams into a flow region with an initial base area, Figs. 1 and 2, this is equivalent to the instantaneous introduction of a disparity between the sum of all stream areas and the total internal geometric cross-sectional area. In addition, the model must treat the supersonic expansion of the initially subsonic mixed stream [the $O_2(a^1\Delta)$ stream in the COIL case] which is known to occur downstream of an aerodynamic throat created by the expansion of the higher pressure unmixed streams. Therefore a method consistent with other applicable physical laws by which the desired flow conditions are achieved via asymptotic apportionment of the base area was required.

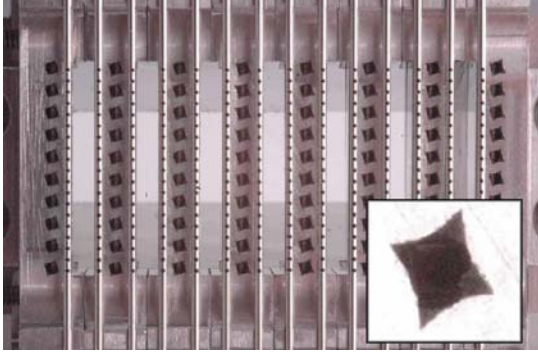


Figure 1 Photograph of ejector mixing nozzle hardware used by [King, 2010] with alternating columns of “starlet” ejectors (see inset), I_2 injector tubes, O_2 slot flow, and base area around the ejectors. Flow direction out of paper.

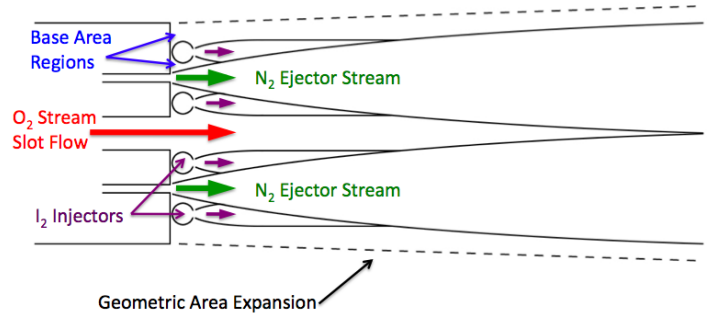


Figure 2 Schematic of 1-D flow simulation for BLAZE-IV modeling showing multi-stream mixing and base regions, but loss of three-dimensionality. Note that the diagram only shows a single slot, but the whole system is treated in the computations.

As the model treats gas stream-wise velocity, density, pressure, temperature, and flow area in addition to the n chemical specie mole fractions as dependent variables and uses the coupled linearized momentum, continuity, energy, state, and n molecular continuity equations to solve for dependent variable stream-wise derivatives, a fifth fluids equation is required to close the constructed linear system. In the standard model, the derivative of the i^{th} stream area is assumed to be equal to the derivative of the geometric area multiplied by a factor f_i that apportions the geometric area derivative amongst all streams

$$\left. \frac{\partial A}{\partial x} \right|_i \equiv \frac{\partial}{\partial x} [A_{GEOM}(x)] \cdot f_i \quad (1)$$

where the instantaneous f_i are fully determined by the instantaneous stream areas and rates of stream to stream mass exchange resulting from mixing. Several methods for treating the base area region were tested and the specification of the stream Mach number derivatives was found to be effective. In the modified model, Eq. (1) is replaced by

$$\left. \frac{\partial M}{\partial x} \right|_{i=0} = \frac{\partial}{\partial x} \left(\left. \frac{V}{\sqrt{\gamma RT}} \right|_{i=0} \right) = \frac{M_{TARGET} \Big|_{MIXED} - M_i}{h \Big|_{MIXED}} \quad (2)$$

$$\left. \frac{\partial M}{\partial x} \right|_{i \neq 0} = \frac{\partial}{\partial x} \left(\left. \frac{V}{\sqrt{\gamma RT}} \right|_{i \neq 0} \right) = \frac{M_{TARGET} \Big|_{UNMIXED} - M_i}{h \Big|_{UNMIXED}}$$

where M_{TARGET} is a target Mach number to be reached over a characteristic length h (note that the streams are indexed such that the 0^{th} stream corresponds to the single mixed stream, and the equations are constructed such that different target Mach numbers and characteristic lengths may be specified for the mixed and unmixed streams). Further note that to ensure numerical stability and solution “smoothness” the maximum step size used in the axial Newton integration must be set to a value much less than h . Evaluating the derivative in Eq. (2) provides a linear partial differential equation that is appropriately a function of the dependent fluid-dynamic variables and their derivatives.

$$\left[\left. \frac{1}{\sqrt{\gamma RT}} \left(\frac{\partial V}{\partial x} - \frac{V}{2T} \frac{\partial T}{\partial x} \right) \right] \Big|_{i=0} = \frac{M_{TARGET} \Big|_{MIXED} - M_i}{h \Big|_{MIXED}} \quad (3)$$

$$\left[\left. \frac{1}{\sqrt{\gamma RT}} \left(\frac{\partial V}{\partial x} - \frac{V}{2T} \frac{\partial T}{\partial x} \right) \right] \Big|_{i \neq 0} = \frac{M_{TARGET} \Big|_{UNMIXED} - M_i}{h \Big|_{UNMIXED}}$$

Test cases (not shown for brevity) have demonstrated that solutions obtained using the solution method including Eq. (4) typically do not violate the geometric area constraint (constraint that the sum of all streams’ cross-

sectional areas is not greater than the geometric system cross-sectional area) for reasonable target Mach numbers, and if the geometric area constraint is violated, the discrepancy is not overwhelming. Therefore it is possible to include an additional requirement that the geometric area constraint not be violated without significantly affecting the resulting solutions or the tendency of the solutions to converge to reasonable specified target Mach numbers. As the solution method described above is used to determine the instantaneous fluid–dynamic derivative vector,

$$\left. \frac{\partial}{\partial x} \{V, \rho, P, T, A\}^T \right|_i \quad (4)$$

if the determined fluid–dynamic derivative vector is such that

$$\left. \frac{\partial A}{\partial x} \right|_i > \frac{A_{GEOM} - \sum_{i=0}^n A_i}{h_{INT}} + \frac{\partial A_{GEOM}}{\partial x} \quad (5)$$

indicating that within the next integration step the geometric area criterion will be violated, the linear system solution process is repeated with Eq. (3) replaced by

$$\left. \frac{\partial A}{\partial x} \right|_i = \frac{A_{GEOM} - \sum_{i=0}^n A_i}{h_{INT}} + \frac{\partial A_{GEOM}}{\partial x} \quad (6)$$

which ensures that the solution will satisfy the geometric area criterion. To ensure that the behavior of the individual stream Mach numbers is monotonic in the region immediately following the aerodynamic throat (noting that thermal choking may still occur much further downstream), when the condition determined by Eq. (5) is violated, the mixed and unmixed target Mach numbers are reset to match the instantaneous mixed stream Mach number.

The calculations presented in this section assume a kinetic set comprised of the 31 species: $O_2(^3X)$, $O_2(^3X, v=1)$, $O_2(^3X, v=2)$, $O_2(^3X, v=3)$, $O_2(^3X, v=4)$, $O_2(^3X, v=5)$, $O_2(a^1\Delta)$, $O_2(a^1\Delta, v=1)$, $O_2(a^1\Delta, v=2)$, $O_2(a^1\Delta, v=3)$, $O_2(a^1\Delta, v=4)$, $O_2(a^1\Delta, v=5)$, $O_2(b^1\Sigma)$, $O_2(b^1\Sigma, v=1)$, $O_2(b^1\Sigma, v=2)$, $O_2(b^1\Sigma, v=3)$, $O_2(b^1\Sigma, v=4)$, $O_2(b^1\Sigma, v=5)$, Cl_2 , Cl , ICl , H_2O , N_2 , He , I_2 , $I_2(v=20)$, $I_2(^3\Pi_{2U})$, $I_2(^3\Pi_{1U})$, $I_2(^3\Pi_{0+U})$, $I(^2P_{3/2})$, and $I(^2P_{1/2})$. The calculations also assume a kinetic set comprised of 122 kinetic reactions (not including equilibrium determined reverse reactions), Table 1. Note that the reaction set is based on the standard COIL reaction set but includes more substantial vibrational kinetics and a more advanced I_2 dissociation mechanism as described by [Waichman, 2007]. Note that a further modified mechanism was implemented more recently by Azyazov et al. [Azyazov, 2009] that includes individual vibrational states of I_2 ; we recommend that this mechanism be examined in future detailed modeling studies.

Table 1 Reaction set used in BLAZE-IV calculations presented in the current section. Note that reaction rate units are $cm^3/molecule\cdot s$ and $cm^6/molecule^2\cdot s$ for two and three-body reactions respectively. († Denotes a reaction and rate derived from a similar reaction. → and ↔ Denote one-way and reversible reactions respectively).

<i>k</i>	<i>Reaction</i>	<i>Rate</i>	<i>Ref.</i>
1	$2 O_2(a^1\Delta) \rightarrow 2 O_2(^3X)$	1.69×10^{-17}	Perram, 1988
2	$2 O_2(a^1\Delta) \rightarrow 2 O_2(a^1\Delta, v=3)$	1.7×10^{-17}	Waichman, 2007
3	$2 O_2(a^1\Delta) \rightarrow O_2(^3X) + O_2(b^1\Sigma)$	$9.8 \times 10^{-28} T^{3.8} \exp(700/T)$	Perram, 1988
4	$2 O_2(a^1\Delta) \rightarrow O_2(^3X) + O_2(b^1\Sigma, v=2)$	$9.5 \times 10^{-28} T^{3.8} \exp(700/T)$	Waichman, 2007
5	$2 O_2(a^1\Delta, v=1) \leftrightarrow O_2(a^1\Delta) + O_2(a^1\Delta, v=2)$	2×10^{-13}	†
6	$2 O_2(a^1\Delta, v=3) \leftrightarrow O_2(a^1\Delta, v=2) + O_2(a^1\Delta, v=4)$	2.6×10^{-13}	†
7	$2 O_2(a^1\Delta, v=4) \leftrightarrow O_2(a^1\Delta, v=3) + O_2(a^1\Delta, v=5)$	2.6×10^{-13}	†
8	$2 O_2(b^1\Sigma) \rightarrow O_2(^3X) + O_2(a^1\Delta)$	5.6×10^{-17}	Atkinson, 1977
9	$2 O_2(b^1\Sigma, v=1) \leftrightarrow O_2(b^1\Sigma) + O_2(b^1\Sigma, v=2)$	2×10^{-13}	†
10	$2 O_2(b^1\Sigma, v=3) \leftrightarrow O_2(b^1\Sigma, v=2) + O_2(b^1\Sigma, v=4)$	2.6×10^{-13}	†
11	$2 O_2(b^1\Sigma, v=4) \leftrightarrow O_2(b^1\Sigma, v=3) + O_2(b^1\Sigma, v=5)$	2.6×10^{-13}	†

12	$2 \text{O}_2(^3\text{X}, v=1) \leftrightarrow \text{O}_2(^3\text{X}) + \text{O}_2(^3\text{X}, v=2)$	2×10^{-13}	Waichman, 2007
13	$2 \text{O}_2(^3\text{X}, v=3) \leftrightarrow \text{O}_2(^3\text{X}, v=2) + \text{O}_2(^3\text{X}, v=4)$	2.6×10^{-13}	†
14	$2 \text{O}_2(^3\text{X}, v=4) \leftrightarrow \text{O}_2(^3\text{X}, v=3) + \text{O}_2(^3\text{X}, v=5)$	2.6×10^{-13}	†
15	$\text{Cl} + \text{I}_2 \rightarrow \text{I}(^2\text{P}_{3/2}) + \text{ICl}$	1.99×10^{-10}	Perram, 1988
16	$\text{Cl} + \text{ICl} \rightarrow \text{Cl}_2 + \text{I}(^2\text{P}_{3/2})$	8.01×10^{-12}	Perram, 1988
17	$\text{Cl}_2 + \text{I}(^2\text{P}_{1/2}) \rightarrow \text{Cl} + \text{ICl}$	5.5×10^{-15}	Perram, 1988
18	$\text{Cl}_2 + \text{I}(^2\text{P}_{1/2}) \rightarrow \text{Cl}_2 + \text{I}(^2\text{P}_{3/2})$	8.01×10^{-15}	Perram, 1988
19	$\text{Cl}_2 + \text{I}_2(v=20) \rightarrow \text{Cl}_2 + \text{I}_2$	6.3×10^{-12}	Heaven, 1995
20	$\text{Cl}_2 + \text{O}_2(a^1\Delta) \rightarrow \text{Cl}_2 + \text{O}_2(^3\text{X})$	6×10^{-18}	Perram, 1988
21	$\text{Cl}_2 + \text{O}_2(b^1\Sigma) \rightarrow \text{Cl}_2 + \text{O}_2(a^1\Delta)$	1.99×10^{-15}	Perram, 1988
22	$\text{H}_2\text{O} + \text{I}(^2\text{P}_{1/2}) \rightarrow \text{H}_2\text{O} + \text{I}(^2\text{P}_{3/2})$	2.11×10^{-12}	Perram, 1988
23	$\text{H}_2\text{O} + \text{I}_2(v=20) \rightarrow \text{H}_2\text{O} + \text{I}_2$	1.69×10^{-11}	Heaven, 1995
24	$\text{H}_2\text{O} + \text{O}_2(a^1\Delta) \rightarrow \text{H}_2\text{O} + \text{O}_2(^3\text{X})$	4×10^{-18}	Perram, 1988
25	$\text{H}_2\text{O} + \text{O}_2(a^1\Delta, v=1) \rightarrow \text{H}_2\text{O} + \text{O}_2(a^1\Delta)$	1.7×10^{-12}	Waichman, 2007
26	$\text{H}_2\text{O} + \text{O}_2(a^1\Delta, v=2) \leftrightarrow \text{H}_2\text{O} + \text{O}_2(a^1\Delta, v=1)$	1.7×10^{-12}	†
27	$\text{H}_2\text{O} + \text{O}_2(a^1\Delta, v=3) \leftrightarrow \text{H}_2\text{O} + \text{O}_2(a^1\Delta, v=2)$	1.7×10^{-12}	†
28	$\text{H}_2\text{O} + \text{O}_2(a^1\Delta, v=4) \leftrightarrow \text{H}_2\text{O} + \text{O}_2(a^1\Delta, v=3)$	1.7×10^{-12}	†
29	$\text{H}_2\text{O} + \text{O}_2(a^1\Delta, v=5) \leftrightarrow \text{H}_2\text{O} + \text{O}_2(a^1\Delta, v=4)$	1.7×10^{-12}	†
30	$\text{H}_2\text{O} + \text{O}_2(b^1\Sigma) \rightarrow \text{H}_2\text{O} + \text{O}_2(a^1\Delta)$	6.71×10^{-12}	Perram, 1988
31	$\text{H}_2\text{O} + \text{O}_2(b^1\Sigma) \leftrightarrow \text{H}_2\text{O} + \text{O}_2(a^1\Delta, v=3)$	6.7×10^{-12}	Waichman, 2007
32	$\text{H}_2\text{O} + \text{O}_2(b^1\Sigma, v=1) \leftrightarrow \text{H}_2\text{O} + \text{O}_2(b^1\Sigma)$	1.7×10^{-12}	†
33	$\text{H}_2\text{O} + \text{O}_2(b^1\Sigma, v=2) \leftrightarrow \text{H}_2\text{O} + \text{O}_2(b^1\Sigma, v=1)$	1.7×10^{-12}	†
34	$\text{H}_2\text{O} + \text{O}_2(b^1\Sigma, v=3) \leftrightarrow \text{H}_2\text{O} + \text{O}_2(b^1\Sigma, v=2)$	1.7×10^{-12}	†
35	$\text{H}_2\text{O} + \text{O}_2(b^1\Sigma, v=4) \leftrightarrow \text{H}_2\text{O} + \text{O}_2(b^1\Sigma, v=3)$	1.7×10^{-12}	†
36	$\text{H}_2\text{O} + \text{O}_2(b^1\Sigma, v=5) \leftrightarrow \text{H}_2\text{O} + \text{O}_2(b^1\Sigma, v=4)$	1.7×10^{-12}	†
37	$\text{H}_2\text{O} + \text{O}_2(^3\text{X}, v=1) \leftrightarrow \text{H}_2\text{O} + \text{O}_2(^3\text{X})$	1.7×10^{-12}	Waichman, 2007
38	$\text{H}_2\text{O} + \text{O}_2(^3\text{X}, v=2) \leftrightarrow \text{H}_2\text{O} + \text{O}_2(^3\text{X}, v=1)$	1.7×10^{-12}	†
39	$\text{H}_2\text{O} + \text{O}_2(^3\text{X}, v=3) \leftrightarrow \text{H}_2\text{O} + \text{O}_2(^3\text{X}, v=2)$	1.7×10^{-12}	†
40	$\text{H}_2\text{O} + \text{O}_2(^3\text{X}, v=4) \leftrightarrow \text{H}_2\text{O} + \text{O}_2(^3\text{X}, v=3)$	1.7×10^{-12}	†
41	$\text{H}_2\text{O} + \text{O}_2(^3\text{X}, v=5) \leftrightarrow \text{H}_2\text{O} + \text{O}_2(^3\text{X}, v=4)$	1.7×10^{-12}	†
42	$\text{He} + 2 \text{I}(^2\text{P}_{3/2}) \rightarrow \text{He} + \text{I}_2$	3.81×10^{-33}	Busch, 1978
43	$\text{He} + \text{I}(^2\text{P}_{1/2}) \rightarrow \text{He} + \text{I}(^2\text{P}_{3/2})$	5×10^{-18}	Perram, 1988
44	$\text{He} + \text{I}_2(v=20) \rightarrow \text{He} + \text{I}_2$	9.8×10^{-12}	Heaven, 1995
45	$\text{He} + \text{O}_2(a^1\Delta) \rightarrow \text{He} + \text{O}_2(^3\text{X})$	8.01×10^{-21}	Perram, 1988
46	$\text{He} + \text{O}_2(b^1\Sigma) \rightarrow \text{He} + \text{O}_2(a^1\Delta)$	1×10^{-17}	Perram, 1988
47	$\text{He} + \text{O}_2(^3\text{X}, v=1) \leftrightarrow \text{He} + \text{O}_2(^3\text{X})$	1.3×10^{-13}	Atkinson, 1977
48	$\text{He} + \text{O}_2(^3\text{X}, v=2) \leftrightarrow \text{He} + \text{O}_2(^3\text{X}, v=1)$	1.3×10^{-13}	†
49	$\text{He} + \text{O}_2(^3\text{X}, v=3) \leftrightarrow \text{He} + \text{O}_2(^3\text{X}, v=2)$	1.3×10^{-13}	†
50	$\text{He} + \text{O}_2(^3\text{X}, v=4) \leftrightarrow \text{He} + \text{O}_2(^3\text{X}, v=3)$	1.3×10^{-13}	†
51	$\text{He} + \text{O}_2(^3\text{X}, v=5) \leftrightarrow \text{He} + \text{O}_2(^3\text{X}, v=4)$	1.3×10^{-13}	†
52	$\text{I}(^2\text{P}_{3/2}) + \text{I}(^2\text{P}_{1/2}) + \text{I}_2 \leftrightarrow \text{I}_2 + 2 \text{I}(^2\text{P}_{3/2})$	3.61×10^{-30}	Perram, 1988
53	$\text{I}(^2\text{P}_{3/2}) + \text{I}(^2\text{P}_{1/2}) + \text{I}_2 \leftrightarrow \text{I}_2 + \text{I}_2(^3\Pi_{0+U})$	3.61×10^{-30}	Perram, 1988
54	$\text{I}(^2\text{P}_{3/2}) + \text{I}(^2\text{P}_{1/2}) \rightarrow 2 \text{I}(^2\text{P}_{3/2})$	1.69×10^{-13}	Perram, 1988
55	$\text{I}(^2\text{P}_{3/2}) + \text{O}_2(a^1\Delta) \rightarrow \text{I}(^2\text{P}_{3/2}) + \text{O}_2(^3\text{X})$	1×10^{-15}	Perram, 1988
56	$\text{I}(^2\text{P}_{3/2}) + \text{O}_2(a^1\Delta) \rightarrow \text{I}(^2\text{P}_{1/2}) + \text{O}_2(^3\text{X})$	$6.29 \times 10^{-12} \text{T}^{0.5}$	Van Marter, 1998
57	$\text{I}(^2\text{P}_{1/2}) + \text{I}_2 \rightarrow \text{I}(^2\text{P}_{3/2}) + \text{I}_2(v=20)$	$1.4 \times 10^{-13} \exp(1600/\text{T})$	Perram, 1988
58	$\text{I}(^2\text{P}_{1/2}) + \text{ICl} \rightarrow \text{Cl} + \text{I}_2$	1.5×10^{-11}	Perram, 1988
59	$\text{I}(^2\text{P}_{1/2}) + \text{N}_2 \rightarrow \text{I}(^2\text{P}_{3/2}) + \text{N}_2$	6.5×10^{-17}	Deakin, 1972
60	$\text{I}(^2\text{P}_{1/2}) + \text{O}_2(^3\text{X}) \rightarrow \text{I}(^2\text{P}_{3/2}) + \text{O}_2(^3\text{X})$	3.5×10^{-16}	Perram, 1988
61	$\text{I}(^2\text{P}_{1/2}) + \text{O}_2(^3\text{X}) \rightarrow \text{I}(^2\text{P}_{3/2}) + \text{O}_2(a^1\Delta)$	$8.39 \times 10^{-12} \text{T}^{0.5} \exp(-403/\text{T})$	Van Marter, 1998

62	$I(^2P_{1/2}) + O_2(a^1\Delta) \rightarrow I(^2P_{3/2}) + O_2(a^1\Delta)$	1.1×10^{-13}	Perram, 1988
63	$I(^2P_{1/2}) + O_2(a^1\Delta) \rightarrow I(^2P_{3/2}) + O_2(a^1\Delta, v=3)$	1.1×10^{-13}	Waichman, 2007
64	$I(^2P_{1/2}) + O_2(a^1\Delta) \rightarrow I(^2P_{3/2}) + O_2(b^1\Sigma)$	$4 \times 10^{-24} T^{3.8} \exp(700/T)$	Perram, 1988
65	$I(^2P_{1/2}) + O_2(a^1\Delta) \rightarrow I(^2P_{3/2}) + O_2(b^1\Sigma, v=2)$	$4 \times 10^{-24} T^{3.8} \exp(700/T)$	Waichman, 2007
66	$I_2 + 2 I(^2P_{3/2}) \rightarrow 2 I_2$	3.61×10^{-30}	Perram, 1988
67	$I_2 + O_2(a^1\Delta) \rightarrow I_2 + O_2(^3X)$	5×10^{-16}	Han, 2003
68	$I_2 + O_2(a^1\Delta) \rightarrow I_2(v=20) + O_2(^3X)$	7.01×10^{-15}	Perram, 1988
69	$I_2 + O_2(a^1\Delta, v=1) \rightarrow I_2(^3\Pi_{2U}) + O_2(^3X)$	$1.9 \times 10^{-11} \exp(-897/T)$	Waichman, 2007
70	$I_2 + O_2(a^1\Delta, v=2) \rightarrow I_2(^3\Pi_{1U}) + O_2(^3X)$	3×10^{-11}	Waichman, 2007
71	$I_2 + O_2(a^1\Delta, v=3) \rightarrow O_2(^3X) + 2 I(^2P_{3/2})$	1×10^{-11}	Waichman, 2007
72	$I_2 + O_2(b^1\Sigma) \rightarrow I_2 + O_2(^3X)$	6×10^{-12}	Heaven, 1995
73	$I_2 + O_2(b^1\Sigma) \rightarrow I_2 + O_2(a^1\Delta)$	2.31×10^{-11}	Han, 2003
74	$I_2 + O_2(b^1\Sigma) \rightarrow I_2(^3\Pi_{1U}) + O_2(^3X)$	8×10^{-12}	Waichman, 2007
75	$I_2 + O_2(b^1\Sigma) \rightarrow I_2(^3\Pi_{2U}) + O_2(^3X)$	8×10^{-12}	Waichman, 2007
76	$I_2 + O_2(b^1\Sigma) \rightarrow O_2(^3X) + 2 I(^2P_{3/2})$	2.81×10^{-11}	Heaven, 2005
77	$I_2(^3\Pi_{0+U}) \rightarrow 2 I(^2P_{3/2})$	1×10^6	Perram, 1988
78	$I_2(^3\Pi_{1U}) + O_2(a^1\Delta) \rightarrow O_2(^3X) + 2 I(^2P_{3/2})$	3×10^{-10}	Waichman, 2007
79	$I_2(^3\Pi_{2U}) + O_2(a^1\Delta) \rightarrow O_2(^3X) + 2 I(^2P_{3/2})$	3×10^{-10}	Waichman, 2007
80	$I_2(v=20) + O_2(^3X) \rightarrow I_2 + O_2(^3X)$	4.9×10^{-12}	Heaven, 1995
81	$I_2(v=20) + O_2(a^1\Delta) \rightarrow O_2(^3X) + 2 I(^2P_{3/2})$	3.01×10^{-10}	Perram, 1988
82	$N_2 + I_2(v=20) \rightarrow N_2 + I_2$	8.17×10^{-12}	Heaven, 1996
83	$N_2 + 2 I(^2P_{3/2}) \rightarrow N_2 + I_2$	4.19×10^{-32}	Busch, 1978
84	$N_2 + O_2(a^1\Delta) \rightarrow N_2 + O_2(^3X)$	1.4×10^{-19}	Atkinson, 1977
85	$N_2 + O_2(b^1\Sigma) \rightarrow N_2 + O_2(^3X)$	1.99×10^{-16}	Atkinson, 1977
86	$N_2 + O_2(b^1\Sigma) \rightarrow N_2 + O_2(a^1\Delta)$	1.79×10^{-15}	Atkinson, 1977
87	$O_2(^3X) + 2 I(^2P_{3/2}) \rightarrow I_2 + O_2(^3X)$	3.34×10^{-32}	Han, 2003
88	$O_2(^3X) + 2 I(^2P_{3/2}) \rightarrow I_2 + O_2(a^1\Delta)$	3.7×10^{-33}	Han, 2003
89	$O_2(^3X) + O_2(a^1\Delta) \rightarrow 2 O_2(^3X)$	8.21×10^{-19}	Han, 2003
90	$O_2(^3X) + O_2(b^1\Sigma) \rightarrow 2 O_2(^3X)$	5.6×10^{-17}	Atkinson, 1977
91	$O_2(^3X) + O_2(b^1\Sigma) \rightarrow O_2(^3X) + O_2(a^1\Delta)$	3.7×10^{-17}	Han, 2003
92	$O_2(^3X) + O_2(^3X, v=1) \leftrightarrow 2 O_2(^3X)$	4×10^{-14}	Atkinson, 1977
93	$O_2(^3X) + O_2(^3X, v=2) \leftrightarrow O_2(^3X) + O_2(^3X, v=1)$	4×10^{-14}	†
94	$O_2(^3X) + O_2(^3X, v=3) \leftrightarrow O_2(^3X) + O_2(^3X, v=2)$	4×10^{-14}	†
95	$O_2(^3X) + O_2(^3X, v=4) \leftrightarrow O_2(^3X) + O_2(^3X, v=3)$	4×10^{-14}	†
96	$O_2(^3X) + O_2(^3X, v=5) \leftrightarrow O_2(^3X) + O_2(^3X, v=4)$	4×10^{-14}	†
97	$O_2(a^1\Delta) + O_2(^3X, v=1) \leftrightarrow O_2(^3X) + O_2(a^1\Delta, v=1)$	7.9×10^{-11}	Waichman, 2007
98	$O_2(a^1\Delta) + O_2(^3X, v=2) \leftrightarrow O_2(^3X) + O_2(a^1\Delta, v=2)$	7.3×10^{-11}	Waichman, 2007
99	$O_2(a^1\Delta) + O_2(^3X, v=3) \leftrightarrow O_2(^3X) + O_2(a^1\Delta, v=3)$	7×10^{-11}	Waichman, 2007
100	$O_2(a^1\Delta, v=1) + O_2(a^1\Delta, v=2) \leftrightarrow O_2(a^1\Delta) + O_2(a^1\Delta, v=3)$	2.6×10^{-13}	†
101	$O_2(a^1\Delta, v=1) + O_2(a^1\Delta, v=3) \leftrightarrow O_2(a^1\Delta) + O_2(a^1\Delta, v=4)$	2.6×10^{-13}	†
102	$O_2(a^1\Delta, v=1) + O_2(a^1\Delta, v=4) \leftrightarrow O_2(a^1\Delta) + O_2(a^1\Delta, v=5)$	2.6×10^{-13}	†
103	$O_2(a^1\Delta, v=2) + O_2(a^1\Delta, v=2) \leftrightarrow O_2(a^1\Delta, v=1) + O_2(a^1\Delta, v=3)$	2.6×10^{-13}	†
104	$O_2(a^1\Delta, v=2) + O_2(a^1\Delta, v=3) \leftrightarrow O_2(a^1\Delta, v=1) + O_2(a^1\Delta, v=4)$	2.6×10^{-13}	†
105	$O_2(a^1\Delta, v=2) + O_2(a^1\Delta, v=4) \leftrightarrow O_2(a^1\Delta, v=2) + O_2(a^1\Delta, v=5)$	2.6×10^{-13}	†
106	$O_2(a^1\Delta, v=3) + O_2(a^1\Delta, v=4) \leftrightarrow O_2(a^1\Delta, v=2) + O_2(a^1\Delta, v=5)$	2.6×10^{-13}	†
107	$O_2(b^1\Sigma) + O_2(^3X, v=1) \leftrightarrow O_2(^3X) + O_2(b^1\Sigma, v=1)$	2.51×10^{-11}	Waichman, 2007
108	$O_2(b^1\Sigma) + O_2(^3X, v=2) \leftrightarrow O_2(^3X) + O_2(b^1\Sigma, v=2)$	4.73×10^{-12}	Waichman, 2007
109	$O_2(b^1\Sigma, v=1) + O_2(b^1\Sigma, v=2) \leftrightarrow O_2(b^1\Sigma) + O_2(b^1\Sigma, v=3)$	2.6×10^{-13}	†
110	$O_2(b^1\Sigma, v=1) + O_2(b^1\Sigma, v=3) \leftrightarrow O_2(b^1\Sigma) + O_2(b^1\Sigma, v=4)$	2.6×10^{-13}	†
111	$O_2(b^1\Sigma, v=1) + O_2(b^1\Sigma, v=4) \leftrightarrow O_2(b^1\Sigma) + O_2(b^1\Sigma, v=5)$	2.6×10^{-13}	†

112	$O_2(b^1\Sigma, v=2) + O_2(b^1\Sigma, v=2) \leftrightarrow O_2(b^1\Sigma, v=1) + O_2(b^1\Sigma, v=3)$	2.6×10^{-13}	†
113	$O_2(b^1\Sigma, v=2) + O_2(b^1\Sigma, v=3) \leftrightarrow O_2(b^1\Sigma, v=1) + O_2(b^1\Sigma, v=4)$	2.6×10^{-13}	†
114	$O_2(b^1\Sigma, v=2) + O_2(b^1\Sigma, v=4) \leftrightarrow O_2(b^1\Sigma, v=1) + O_2(b^1\Sigma, v=5)$	2.6×10^{-13}	†
115	$O_2(b^1\Sigma, v=3) + O_2(b^1\Sigma, v=4) \leftrightarrow O_2(b^1\Sigma, v=2) + O_2(b^1\Sigma, v=5)$	2.6×10^{-13}	†
116	$O_2(^3X, v=1) + O_2(^3X, v=2) \leftrightarrow O_2(^3X) + O_2(^3X, v=3)$	2.6×10^{-13}	Waichman, 2007
117	$O_2(^3X, v=1) + O_2(^3X, v=3) \leftrightarrow O_2(^3X) + O_2(^3X, v=4)$	2.6×10^{-13}	†
118	$O_2(^3X, v=1) + O_2(^3X, v=4) \leftrightarrow O_2(^3X) + O_2(^3X, v=5)$	2.6×10^{-13}	†
119	$O_2(^3X, v=2) + O_2(^3X, v=2) \leftrightarrow O_2(^3X, v=1) + O_2(^3X, v=3)$	2.6×10^{-13}	†
120	$O_2(^3X, v=2) + O_2(^3X, v=3) \leftrightarrow O_2(^3X, v=1) + O_2(^3X, v=4)$	2.6×10^{-13}	†
121	$O_2(^3X, v=2) + O_2(^3X, v=4) \leftrightarrow O_2(^3X, v=1) + O_2(^3X, v=5)$	2.6×10^{-13}	†
122	$O_2(^3X, v=3) + O_2(^3X, v=4) \leftrightarrow O_2(^3X, v=2) + O_2(^3X, v=5)$	2.6×10^{-13}	†

III. Baseline Calculations

The $N_2 = 270$ mmol/s tertiary flow rate baseline case calculations illustrate the expansion of the various mixing streams into the base area region, Fig. 3. The primary O_2 /mixed area is equal to that of the primary plenum area at the nozzle exit plane (N.E.P.) and gradually expands to fill the majority of the lasing duct while converging to match the sum of all stream areas as mixing completes, Fig. 3. Mixing of the secondary and tertiary stream mass fluxes into the primary mixed stream is presented in Fig. 4. Note that mixing model input parameters (and therefore the modeled mixing rates) were baselined to the system configuration and performance described in [Nikolaev, 2002] and [Hager, 2003] by assuming that the optical axis location used in those studies was near optimum for the achieved mixing performance. Also note that the total gas stream area is slightly less than the geometric area, Fig. 3, due to the inclusion of an estimation of a boundary layer that is consistent with matching the target Mach number in Eq. (3) that effectively reduces the geometric area. The result that the mixing is mostly complete after 2 cm downstream from the N.E.P. appears to be approximately a factor of 2 faster than indicated by PLIF imaging in Ragheb *et al.* [Ragheb, 2010]; this is consistent with other 1D modeling in which it is nearly impossible to match the more detailed aspects of 3D experimental data with a 1D model.

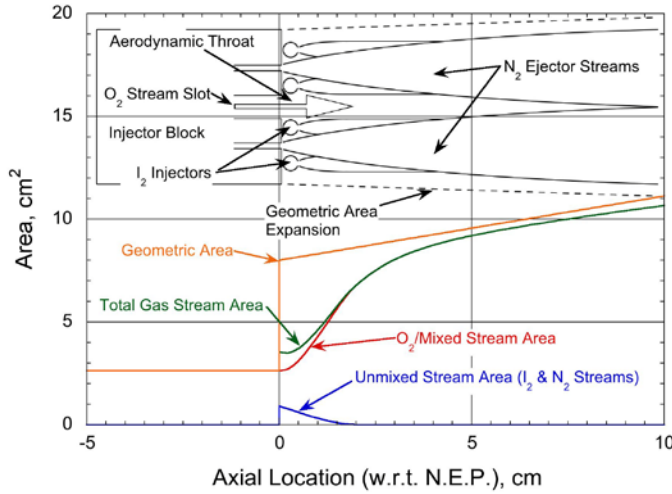


Figure 3 BLAZE-IV calculated stream area for the tertiary $N_2 = 270$ mmol/s zero power case as a function of axial location w.r.t. the nozzle exit plane.

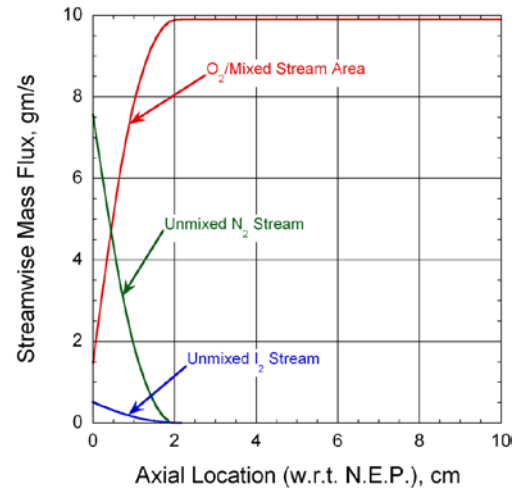


Figure 4 BLAZE-IV calculated stream mass flux for the tertiary $N_2 = 270$ mmol/s zero power case as a function of axial location w.r.t. the nozzle exit plane.

The mixed stream aerodynamic throat and subsequent supersonic expansion to match Mach number data [Nikolaev, 2002] and further supersonic expansion of sonically injected unmixed secondary and tertiary unmixed streams is shown in Fig. 5. Figure 6 illustrates the resulting temperature changes in all streams, and reasonable agreement between predicted mixed stream temperature and data.

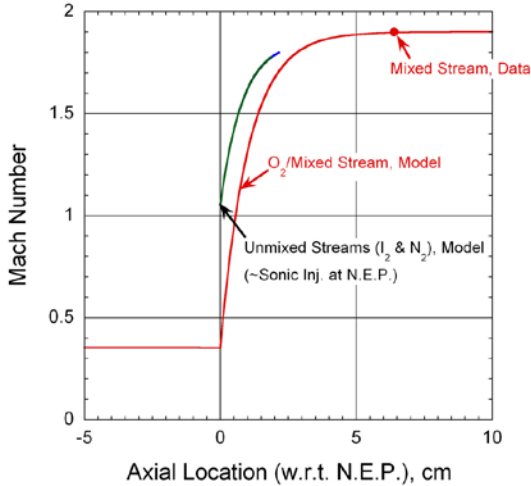


Figure 5 BLAZE-IV calculated stream Mach number for the tertiary $N_2 = 270$ mmol/s zero power case as a function of axial location w.r.t. the nozzle exit plane compared to data [Nikolaev, 2002].

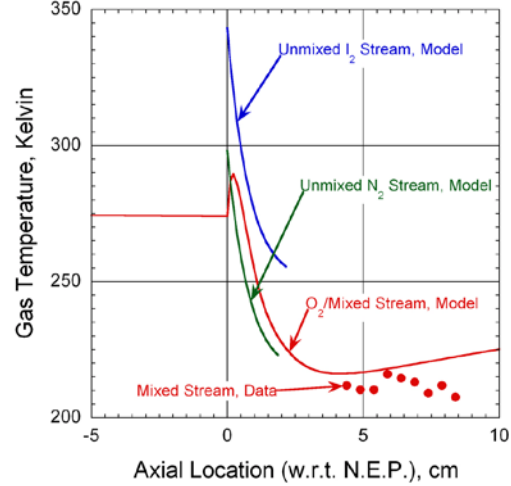


Figure 6 BLAZE-IV calculated stream temperature for the tertiary $N_2 = 270$ mmol/s zero power case as a function of axial location w.r.t. the nozzle exit plane compared to data [Nikolaev, 2002].

The single case calculation presented in Figures 3-6 was repeated assuming a $N_2 = 530$ mmol/s tertiary flow rate. Oxygen plenum pressures of 27.77 and 34.5 Torr were used for $N_2 = 270$ and 530 mmol/s tertiary flow rate cases respectively given data [Nikolaev, 2002] indicating an oxygen plenum pressure variation from 25 to 34.5 Torr over the $N_2 = 160$ to 530 mmol/s tertiary flow rate range and assuming a linear oxygen plenum pressure vs. tertiary flow rate variation. Gas temperature and zero power optical path averaged gain data as a function of tertiary flow rate and axial location with respect to (w.r.t.) the nozzle exit plane were reasonably well modeled, Figs. 7 and 8. The temperature variation as a function of tertiary flow rate is the result of different mixed stream target Mach numbers, 1.9 and 2.3 for the $N_2 = 270$ and 530 mmol/s tertiary flow rate cases respectively, used in the base area expansion model. The target Mach numbers were obtained from data [Nikolaev, 2002]. The larger zero power optical path averaged gain values in the $N_2 = 270$ mmol/s tertiary flow rate case as compared to the $N_2 = 530$ mmol/s case, despite of the lower gas temperatures in the later case, are the result of greater $O_2(a^1\Delta)$ losses in the oxygen plenum upstream of the nozzle exit plane associated with the higher pressures in the $N_2 = 530$ mmol/s case, Fig. 8. Note that for the 530 mmol/s case we are underpredicting the temperature by approximately 15 degrees, Fig. 7, which is the likely reason that we are overpredicting the measured gain, Fig. 8.

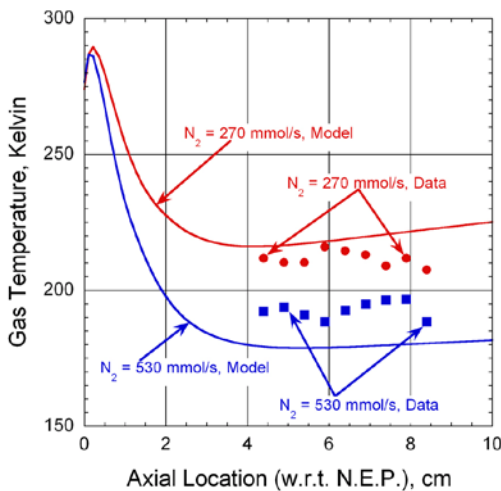


Figure 7 BLAZE-IV calculated mixed stream temperature for the tertiary $N_2 = 270$ and 530 mmol/s zero power cases as a function of axial location w.r.t. the nozzle exit plane compared to data [Nikolaev, 2002].

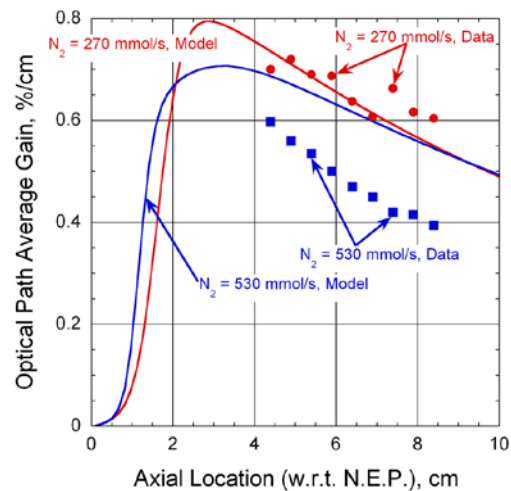


Figure 8 BLAZE-IV calculated mixed stream Mach number for the tertiary $N_2 = 270$ and 530 mmol/s zero power cases as a function of axial location w.r.t. the nozzle exit plane compared to data [Nikolaev, 2002].

A parametric study, based on the $N_2 = 530$ mmol/s tertiary flow rate case, was performed in which the secondary I_2 flow rate was varied over the range of 0 to 1.2 mmol/s with a fixed $N_2 = 11$ mmol/s carrier. Gas temperature at the optical axis location data was reasonably well modeled while zero power optical path averaged gain at the optical axis was slightly over-predicted, while trends as a function of secondary I_2 flow rate were well modeled, Fig. 9.

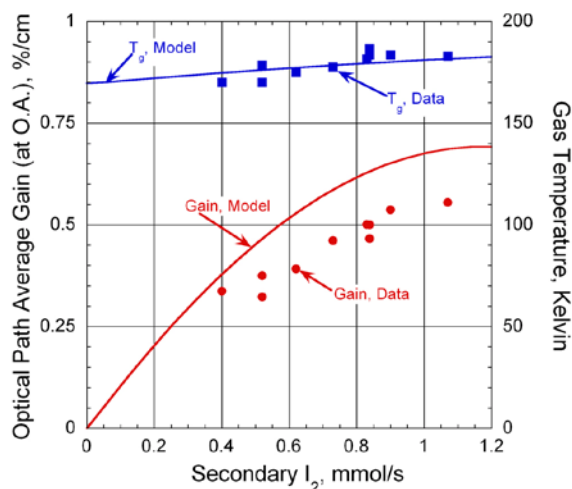


Figure 9 BLAZE-IV calculated optical path average gain and gas temperature at the optical axis for the tertiary $N_2 = 530$ mmol/s zero power case as a function of secondary I_2 flow rate compared to data [Nikolaev, 2002].

Two parametric studies were performed, based on the $N_2 = 270$ and 530 mmol/s tertiary flow rate cases, in which the outcoupler mirror transmissivity was varied over the range of 0 to 6%, Fig. 10. Data as a function of outcoupler transmissivity and tertiary flow rate was reasonably well modeled assuming an outcoupler absorptivity of 0.1% and the optimum outcoupler transmissivity of near 1% from data was well modeled, Fig 10. Two additional parametric studies were performed, based on the $N_2 = 270$ and 530 mmol/s tertiary flow rate cases, in which an added primary stream He diluent was varied over the range of 0 to 40 mmol/s, Fig. 11. Data as a function of primary stream He diluent flow rate and tertiary flow rate was reasonably well modeled, Fig 11. The increase in outcoupled power associated with increased diluent flow rate is the result of smaller primary stream residence times in the oxygen plenum and therefore reduced losses, Fig. 11. The performance of the $N_2 = 530$ mmol/s tertiary flow rate cases rises to match that of the $N_2 = 270$ mmol/s tertiary flow rates cases as the He diluent flow rate approaches 40 mmol/s as the pressure/residence time $O_2(a^1\Delta)$ loss effect is sufficiently mitigated in the higher tertiary flow rate case associated with higher pressures to extract energy at a rate comparable to that of the lower tertiary flow rate case, Fig. 11.

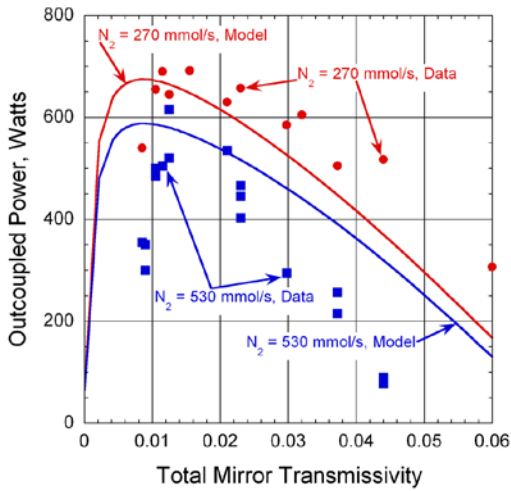


Figure 10 BLAZE-IV calculated outcoupled laser power for the tertiary $N_2 = 270$ and 530 mmol/s cases as a function of outcoupler mirror transmissivity compared to data [Hager, 2003].

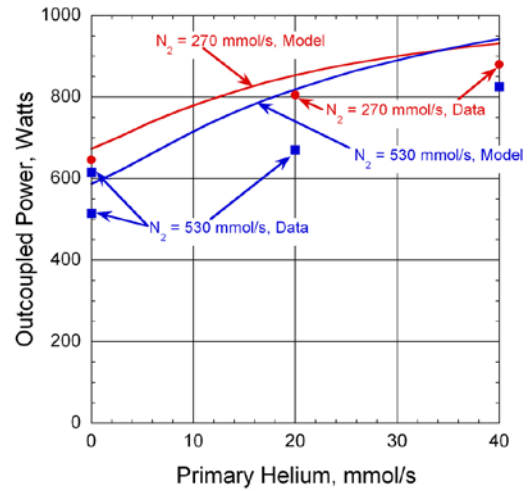


Figure 11 BLAZE-IV calculated outcoupled laser power for the tertiary $N_2 = 270$ and 530 mmol/s cases as a function of primary stream He diluent flow rate compared to data [Hager, 2003].

Figures 3–11 show reasonable agreement between the BLAZE-IV model and experimental data; the qualitative trends are all matched and the quantitative values are acceptably close for the limited dimensionality of the model. This baselining of the model to the data gives us confidence that we can now use the model to investigate trends that we might expect to observe with the faster mixing Starlet ejectors and higher pressure operation.

IV. Parametric Modeling Studies of Enhanced Mixing

A parametric study was performed to illustrate possible performance gains associated with cold tertiary N_2 . As all subsequent parametric studies are intended to illustrate optimum performance conditions, an intermediate study (not shown for brevity) was performed to determine an optimum secondary I_2 flow rate for maximum laser power extraction with the $N_2 = 270$ mmol/s tertiary flow rate case. The optimum secondary I_2 flow rate was determined to be 0.4 mmol/s, corresponding to a reasonable $I_2:O_2$ titration ratio slightly larger than 1%. The parametric study varied the tertiary N_2 temperature over the range of 150 to 300 K. The calculations predict a ~25% improvement associated with cooling the N_2 tertiary stream from 300 to 150 K, and a significant reduction in unextracted $O_2(a^1\Delta)$ power flux, Fig. 12.

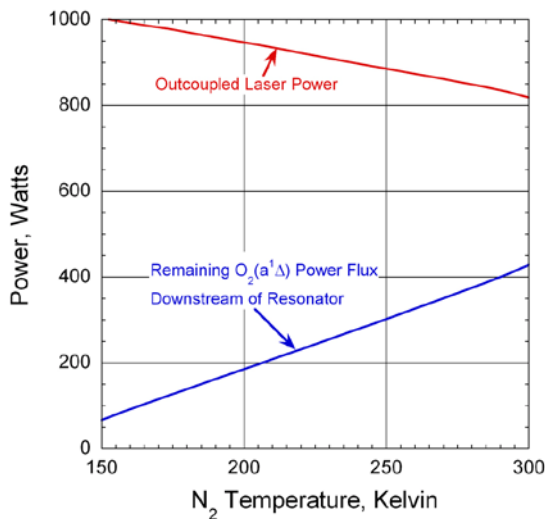


Figure 12 BLAZE-IV calculated outcoupled laser power and $O_2(a^1\Delta)$ power flux remaining downstream of the resonator for the secondary $I_2=0.4$ mmol/s, tertiary $N_2 = 270$ mmol/s case as a function of tertiary N_2 temperature.

Another parametric study was performed in which possible performance gains associated with improved mixing were modeled by applying a varying multiplier to the diffusion coefficients used to determine the secondary I₂ stream mixing rate. Given that in the system presently under consideration, the length over which the bulk of the secondary I₂ stream is mixed with the primary stream is of primary importance rather than the length over which complete mixing occurs, a method for characterizing this length was sought. As the mass flux in a given unmixed stream as a function of axial location tends to follow an exponential decay, an exponential decay fit of the form

$$\dot{m}_i(x) = a + b \exp(-x/\tau) \quad (7)$$

where $m_i(x)$ is the mass flux in the i^{th} unmixed stream, and a , b , and τ are constants, was applied to the predicted mass flux decay and the constant τ may be considered a characteristic mixing length. A parametric study was performed that varied the secondary I₂ stream characteristic mixing length over the range of ~0.5 to ~20 cm for the secondary I₂ = 0.4 mmol/s, tertiary N₂ = 270 mmol/s case, Fig. 13. Calculations indicate that performance increases resulting from improved I₂ mixing are possible beyond what is thought to have already been achieved, Fig. 13; e.g., the modeling predicts that approximately a 10% increase in outcoupled power can be obtained by reducing the characteristic mixing length (faster mixing) from 6 cm down to 2-3 cm. Furthermore, improved mixing performance will shorten the optimum separation between the nozzle exit plane and the optical axis thereby enabling improved performance by reducing kinetic losses (such as the pooling loss). Further parametric studies in which the characteristic I₂ mixing length for the secondary I₂ = 0.4 mmol/s, tertiary N₂ = 270 mmol/s case was varied were performed for system configurations with both the baseline optical axis location and an optical axis location such that there is 1 cm of separation between the upstream edge of the optical axis and the nozzle exit plane, each for cases where the tertiary N₂ stream is at room temperature and cooled 150 K. Calculations indicate that even further performance increases beyond those indicated by Fig. 13 may be achieved via improved secondary I₂ stream mixing used in conjunction with a cooled tertiary flow and an optimized optical axis location, Fig. 14. For the case of cooled N₂ ejector flow (150 K) and an optical axis 3.5 cm downstream from the N.E.P., the performance was approximately 1100 W versus 790 W in the baseline case, a 39% increase.

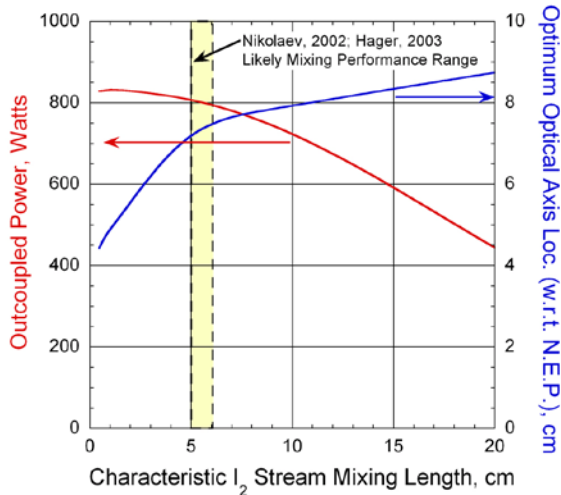


Figure 13 BLAZE-IV calculated outcoupled laser power and optimum optical axis location for the secondary I₂=0.4 mmol/s, tertiary N₂ = 270 mmol/s case as a function of secondary I₂ stream characteristic mixing length.

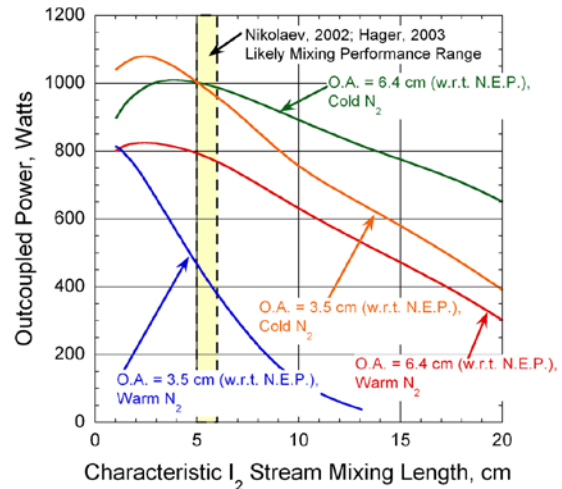


Figure 14 BLAZE-IV calculated outcoupled laser power for the secondary I₂=0.4 mmol/s, tertiary N₂ = 270 mmol/s case as a function of secondary I₂ stream characteristic mixing length, optical axis location, and tertiary N₂ temperature.

Experiments by Nikolaev *et al.* [Nikolaev, 2002] showed that it was possible to achieve in excess of 200 Torr of total pressure recovery. As such, a parametric study with BLAZE-IV was performed in which the tertiary N₂ flow rate was varied over the range of 200 to 1000 mmol/s for the previously modeled system, Fig. 15. Calculations indicate that the specified total pressure target of > 200 Torr should be achievable with on the order of 700 mmol/s of tertiary N₂. Two different transition duct lengths (8" and 12") were investigated for determining the effects of pooling loss on the system performance. The total pressure of the flow is approximately the same regardless of the length of the transition duct, Fig. 15.

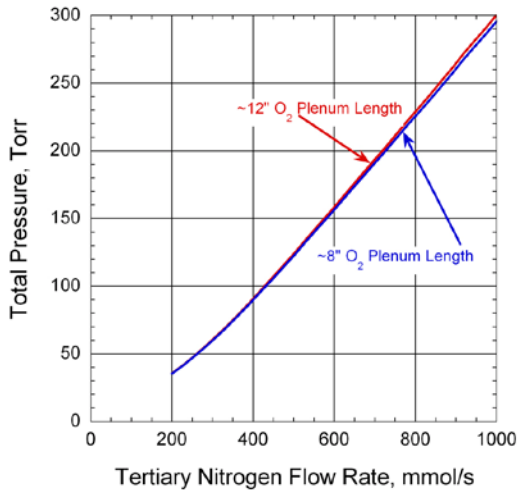


Figure 15 BLAZE-IV calculated total pressure at the downstream edge of the laser resonator for the secondary $I_2=0.4$ mmol/s case as a function of tertiary N_2 flow rate and primary O_2 plenum length.

In a further performance study, the predicted laser chemical efficiency was plotted as a function of total pressure in the lasing duct at the downstream edge of the optical resonator to illustrate the relatively high performance predicted to be achievable at higher total pressures, Fig. 16. Further performance improvements at higher total pressures may be achieved by reducing the travel distance between the $O_2(a^1\Delta)$ generator exit and the nozzle exit plane from 12" to 8", Fig. 16. With reduced primary stream plenum residence times it may be possible to achieve 20% chemical efficiency at 150 to 200 Torr of total mixed stream pressure, Fig. 16. Figure 17 further illustrates total pressure scaling potential using the product of chemical efficiency and total pressure as a scaling performance parameter.

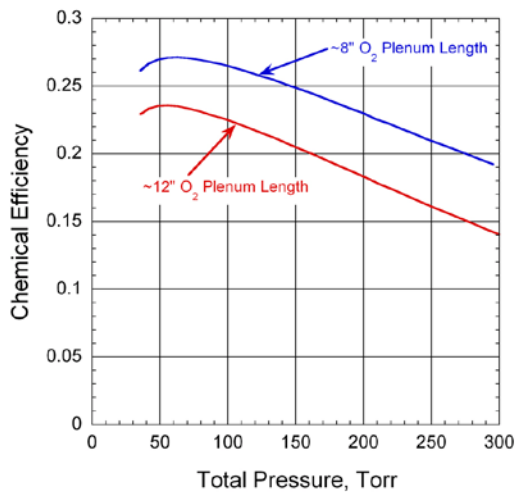


Figure 16 BLAZE-IV laser chemical efficiency for the secondary $I_2=0.4$ mmol/s case as a function of mixed stream total pressure at the downstream edge of the laser resonator and primary O_2 plenum length.

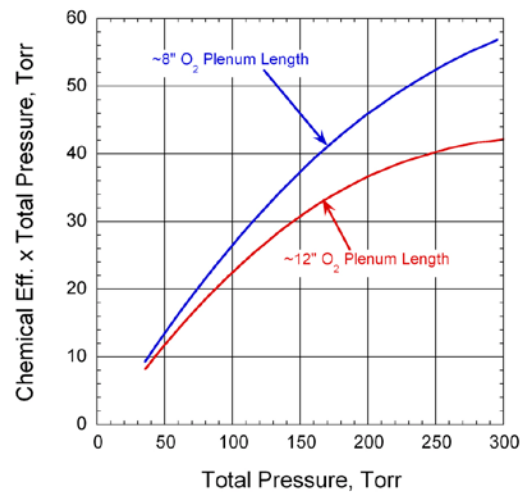


Figure 17 BLAZE-IV laser performance parameter chemical efficiency times total pressure for the secondary $I_2=0.4$ mmol/s case as a function of mixed stream total pressure at the downstream edge of the laser resonator and primary O_2 plenum length.

These BLAZE-IV modeling results support the experimental results from King *et al.* [King, 2010] that higher powers and efficiencies can be obtained with the faster mixing Starlet ejector concept. Further, the modeling indicates that the concept should be viable at high total pressures with 20% chemical efficiency at 250 Torr (Fig. 16) so long as the generator to nozzle plenum region can be minimized in volume.

V. Concluding Remarks

To obtain a better understanding of how much performance enhancement could be expected with increased mixing in high-pressure ejector mixing COIL nozzles and to facilitate a larger parametric study to determine system performance trends we utilized the quasi-1D BLAZE-IV model to simulate existing COIL experiments. While computational fluid dynamic (CFD) computations provide critical detailed information about individual flow fields that cannot be obtained with a model such as BLAZE-IV, the computing time required for these CFD calculations inherently limits the number of such computations that can be performed in a reasonable amount of time. Simulation of COIL ejector mixing nozzle experiments required the development of a BLAZE-IV model component capable of treating the simultaneous expansion of multiple mixing streams into a flow region with an initial base area, which is equivalent to the instantaneous introduction of a disparity between the sum of all stream areas and the total internal geometric cross-sectional area. In addition, the model now treats the supersonic expansion of the initially subsonic mixed stream [the $O_2(a^1\Delta)$ stream in the COIL case] which is known to occur downstream of an aerodynamic throat created by the expansion of the higher pressure unmixed streams. A method consistent with the applicable physical laws by which the desired flow conditions are achieved via asymptotic apportionment of the base area was required.

A Russian design served as our baseline for the BLAZE-IV modeling calculations performed herein and reasonable agreement with the experimental data was obtained with the enhanced version of the quasi-1D BLAZE-IV model for the highly three-dimensional flow fields. Comparisons with experimental data and estimations of performance enhancement with faster mixing are presented. BLAZE-IV modeling supports the experimental results of [King, 2010] that higher powers and efficiencies can be obtained with the faster mixing Starlet ejector concept. Further, the modeling indicates that the concept should be viable at high total pressures with 20% chemical efficiency at 250 Torr so long as the generator to nozzle plenum region can be minimized in volume. Lastly, we suggest that the recent Azyazov et al. [Azyazov, 2009] kinetic mechanism that includes reactions for individual vibrational states of I_2 be investigated in the future to confirm its utility for COIL modeling.

Acknowledgments

This work was supported by the Missile Defense Agency (MDA) and by CU Aerospace internal research and development funds. The authors would like to acknowledge the contributions of: D. King, T. Field, J. Laystrom-Woodard (CU Aerospace); G. Elliott and A. Ragheb (University of Illinois at Urbana-Champaign); R. Driscoll and L. Sentman (consultants); and T. Jones, K. Truesdell, E. Trawinski, and C. Greene (U.S. Air Force).

References

- Atkinson, R., Baulch, D. L., Cox, R. A., Hampson, R. F. Jr., Kerr, J. A., Rossi, M. J., and Troe, J., *J. of Phys and Chem. Ref. Data*, **26**, 3, pp. 550-962 (1997).
- Azyazov, V.N., Pichugin, S. Yu., and Heaven, M.C. (2009). *J. Chem. Phys.*, **130**, 104306.
- Boreysho, A.S., Malkov, V.M., and Savin, A.V. (2009). "High-Power Supersonic Chemical Lasers: Gas-Dynamic Problems of Operation of Mobile Systems with PRS," SPIE Vol. 7131, 713103.
- Busch, G. E., *IEEE J. Quantum. Electron.*, vol. 49, no. 6, pp. 794-796, 1978.
- Carroll, D.L., and Solomon, W.C. (2009). "Iodine Injection, Mixing, and Pressure Recovery," U.S. Prov. Patent # 61/176,135.
- Davis, S.J., Rawlins, W.T., Kessler, W.J., Lee, S., Hunter, A.J.R., and Silva, M.L. (2005). "Next generation diagnostics for COIL: new approaches for measuring critical parameters," SPIE Vol. **5777**, 32-38.
- Deakin, J. J. and Husain, D., *JCS Faraday Trans. II*, vol. 68, pp. 1603-1612, 1972.
- Endo, M., and Walter, R.F. (2007). *Gas Lasers*, CRC Press, New York.
- Hager, G. D., Nikolaev, V. D., Svistun, M. I., and Zagidullin, M. V. (2003). "Lasing Performance of a Chemical Oxygen Iodine Laser (COIL) with Advanced Ejector-Nozzle Banks," *Appl. Phys. A*, **77**, 325-329.
- Han, J., Tinney, S. P., and Heaven, M. C., "I^{*} Kinetics of Relevance to Discharge Driven COIL Systems," Proc. SPIE Vol. 5448, p. 261-268, Sep. 2004.
- Heaven, M. C., "Studies of Energy Transfer Processes of Relevance to Chemically and Optically Pumped Lasers," Air Force Office of Scientific Research, Bolling Air Force Base, Final Rep. AFOSR-TR-95-0012, 1995.
- Heaven, M. C., Private Communication, 1996.
- Heaven, M. C., Private Communication, 2005.
- Khvatov, N.A., Nikolaev, V.D., Svistun, M.I., Zagidullin, M.V., and Hager, G.D. (2002). "Lasing Performance of a Chemical Oxygen Iodine Laser (COIL) with Advanced Ejector Nozzle Banks," SPIE Vol. **4760**, 550.

- King, D.M., Field, T.H., Carroll, D.L., Laystrom-Woodard, J.K., Driscoll, R.J., Sentman, L.H., Ragheb, A.M., Elliott, G.S., and Solomon, W.C. (2010). "Performance of a Multi-Stream Injection COIL with Starlet Ejectors," AIAA Paper 2010-4754.
- Kodymova, J. (2007). "Overview on the chemical oxygen-iodine laser technology," SPIE Vol. **6346**, 634609.
- Madden, T.J., Noren, C.A., Ortiz, T., Wilkinson, M., Klennert, W., Chan, R.W., Behrens, H.W., Decker, R., and Walter, R. (2010). "Experimental and Computational Investigation of a Converging-Diverging Nozzle-Diffuser with Cross Flow Injection," AIAA Paper 2010-1156.
- McDermott, W., Pchelkin, N., Benard, D., and Bousek, R. (1978). "An Electronic Transition Chem. Laser," *Appl. Phys. Lett.* **32**, 469.
- Nikolaev, V., Zagidullin, M., Madden, T., and Hager, G. (2000). "An efficient supersonic COIL with more than 200 torr of total pressure in the active medium," AIAA Paper 2000-2427.
- Nikolaev, V.D., Zagidullin, M.V., Svistun, M. I., Anderson, B. T., Tate, R. F., and Hager, G. D. (2002). "Results of Small-Signal Gain Measurements in a Supersonic Chemical Oxygen Iodine Laser With an Advanced Nozzle Bank." *IEEE Journal of Quantum Electronics*, **38** (5) 421-428.
- Palla, A.D., Carroll, D. L., Verdeyen, J. T., and Solomon, W. C., (2006a) "Mixing Effects in Post-Discharge Modeling of Electric Discharge Oxygen-Iodine Laser Experiments," *Jour. Physics D*, 100, 023117.
- Palla, A. D., Carroll, D. L., Verdeyen, J. T., and Solomon, W. C., (2006b) "Effects of Mixing on Post-Discharge Modeling of ElectricOIL Experiments," *Proc. SPIE*, 6101, 610125.
- Palla, A. D., Zimmerman, J. W., Woodard, B. S., Carroll, D. L., Verdeyen, J. T., Lim, T. C., and Solomon, W. C., (2007a) "Oxygen Discharge and Post-Discharge Kinetics Experiments and Modeling for the Electric Oxygen-Iodine Laser System," *Jour. Phys. Chemistry A*, **111**, 6713-6721.
- Palla, A. D., Zimmerman, J. W., Woodard, B. S., Carroll, D. L., Verdeyen, J. T., Lim, T. C., Rawlins, W. T., Lee, S., Davis, S. J., and Solomon, W. C., (2007b) "ElectricOIL Discharge and Post-Discharge Kinetics Experiments and Modeling," *Proc. SPIE*, 6454, 645401.
- Pannu, S.S., and Johannesen, N. H. (1976). "The Structure of Jets from Notched Nozzles," *J. Fluid Mech.*, **74**, 515.
- Perram, G. P., and Hager, G. D., "The Standard Chemical Oxygen-Iodine Laser Kinetics Package," Air Force Weapons Laboratory, Air Force System Command, Kirtland AFB, NM, Final Rep. AFWL-TR-88-50, 1988.
- Ragheb, A.M., Elliott, G.S., Laystrom-Woodard, J.K., King, D.M., Carroll, D.L., and Solomon, W.C. (2010a). "Low Pressure PLIF Visualization and Mixing Quantification in a Multi-Stream Injection Nozzle," AIAA Paper 2010-1439.
- Ragheb, A.M., Elliott, G.S., Laystrom-Woodard, J.K., King, D.M., Carroll, D.L., and Solomon, W.C. (2010b). "Low Pressure Schlieren Imaging of a Multi-Stream Injection Nozzle," to be presented at AIAA 41st Plasmadynamics and Lasers Conference, Chicago, IL, 28 June – 1 July 2010.
- Rybalkin, V., Katz, A., Barmashenko, B.D., and Rosenwaks, S. (2005). "Parametric study of a highly efficient chemical oxygen-iodine laser with supersonic mixing of iodine and oxygen," *J. Applied Phys.* **98**, 023106.
- Solomon, W.C., Bell Aerospace Textron (1982). "Program for Oxygen-Iodine Supersonic Technology Program, Part III, Section II," Report No. D9299-953003, p. 4.1-21.
- Truesdell, K., Lamberson, S., and Hager, G. (1992). "Phillips Laboratory COIL Technology Overview," AIAA Paper 92-3003.
- Van Marter, T., and Heaven, M. C., (1998). " $I(^2P_{1/2})+O_2$: Studies of Low-Temperature Electronic Energy Transfer and Nuclear Spin-State Changing Collisions," *Jour. Chem. Phys.*, **109**, 21, 9266.
- Vorobieff, P., Truman, C.R., Ragheb, A.M., Elliott, G.S., Laystrom-Woodard, J.K., King, D.M., Carroll, D.L., and Solomon, W.C. (2010). "Mixing enhancement in a multi-stream injection nozzle," submitted to *J. of Experiments in Fluids*.
- Waichman, K., Rybalkin, V., Katz, A., Dahan, Z., Barmashenko, B. D., and Rosenwaks, S., (2007). "Toward Understanding the Dissociation of I₂ in Chemical Oxygen-Iodine Laser: Combined Experimental and Theoretical Studies," *Jour. Appl. Phys.*, **102**, 013108.
- Waichman, K., Barmashenko, B.D., and Rosenwaks, S. (2009). "A computational fluid dynamics simulation of a high pressure ejector COIL and comparison to experiments," SPIE Vol. **7131**, 71310R.
- Yang, T., Dickerson, R.A., Moon, L.F., and Hsia, Y.C. (2000). "High Mach Number, High Pressure Recovery COIL Nozzle Aerodynamic Experiments," AIAA Paper 2000-2425.
- Zagidullin, M.V., Nikolaev, V.D., Khvatov, N.A., and Svistun, M.I. (1998). "The sub- and supersonic COILs driven by jet type singlet oxygen generator," SPIE Vol. **3574**, 246-252.
- Zagidullin, M.V., Nikolaev, V.D., Svistun, M.I., Khvatov, N.A., Hager, G.D., and Madden, T.J. (2001). "Efficient chemical oxygen-iodine laser with a high total pressure of the active medium," *Quantum Electronics*, **31**, 30-34.

- Zagidullin, M.V., Nikolaev, V.D., Svistun, M.I., Khvatov, N.A., and Hager, G.D. (2005). "Characteristics of the gain medium for an ejector COIL with supersonic nozzles for the driver buffer gas," *Applied Phys. A*, **81**, 311.
- Zagidullin, M.V., Nikolaev, V.D., Svistun, M.I., Khvatov, N.A., and Fomin, E.V. (2008). "Diagnostics of an $O_2(^1\Delta)$ Generator Using Multichannel Recording of Oxygen Emission Spectra," *Optics and Spectroscopy*, **105**, 202.